Fourteenth USA/Europe Air Traffic Management Research and Development Seminar (ATM2021)

An Integrated Approach for Dynamic Capacity Management Service in U-space

Yiwen Tang, Yan Xu, Gokhan Inalhan, Antonios Tsourdos
School of Aerospace, Transport and Manufacturing
Cranfield University
Bedford, United Kingdom

***Abstract*—This paper presents an integrated approach for the Dynamic Capacity Management service to be offered in U-space. The approach involves three main threads, including flight planning (demand), airspace configuration (capacity) and demand-capacity balancing (DCB). The flight planning thread produces UAS (unmanned aerial systems) trajectories for each flight that together reflect the estimated traffic demand. The airspace configuration thread defines the fundamental airspace structure and proposes dynamic adjustment schemes that determine the capacity distribution. It also enables the flight planning to reschedule alternative trajectory options to route away from possible congested areas. The last DCB thread takes the previous inputs and then computes for the optimal slot allocation and trajectory selection, as well as the optimal airspace configuration. Simulation case studies have been performed through mimicking a future U-space operating scenario. Results suggest that the integrated approach can achieve the best outcome in almost all the key performance areas than any other cases where only partial functions can be realised.**

***Keywords*—U-space; Dynamic Capacity Management; demand-capacity balancing; flight planning; airspace configuration; UAS traffic management**

I. Introduction

It is envisioned that unmanned aerial systems (UAS) will be part of our future in the sky. The growing market shows significant potential across the world, with demand in Europe estimated in excess of EUR 10 billion annually by 2035 and over EUR 15 billion annually by 2050 [1]. Opening the sky, in particular for Very Low Level (VLL) airspace, to these new entrants means a move from several thousand conventional aircraft in the sky every day to potentially hundreds of thousands of aerial vehicles, including in urban cities where the density and ground risks are expected to be higher. Thus, a dedicated UAS traffic management (UTM) system is in urgent need to achieve the smooth, safe and fair integration of UAS into the airspace.

As the conventional air transportation demand constantly grows, air traffic flow and capacity management (ATFCM), one of the three pillars of ATM, has been playing an increasingly important role. Its main objective is to balance the traffic demand and airspace capacity, in such a way that an early-stage safety net can be built to protect the air traffic control (ATC) from being overloaded. Likewise, the fast growing of UAS demand will eventually approach to the airspace threshold, and thus similar ATFCM initiatives may be also required. According to the U-space Roadmap, a service of Dynamic Capacity Management (DCM) is expected to be achieved at U3 stage [2]. Motivated from that, this paper proposes an approach towards the indicated DCM service, in which a set of functions are enabled encompassing flight planning, slot and trajectory allocation, and capacity optimisation. This integrated approach produces an optimal solution minimising the operational costs while maintaining traffic density under the airspace thresholds.

As previously mentioned, the anticipated DCM service seems to have a high level of similarity to the conventional ATFCM, in the sense of their rationale and methodology. Recent studies have shown this trend as well. For example, [3] presented a formulation of the UAS traffic flow management problem, which can be traced back to a classical ATFCM model. Based on that formulation, the authors further discussed the trade-off between efficiency and fairness, which was also addressed precisely in the ATFCM domain by [4]. As an early effort to incorporate UAS trajectories into airspace and airport resource sharing schemes, [5] proposed a distributed system that would enable autonomous trajectory planning by manned and unmanned aircraft, while optimising system-wide objectives. Another way of modelling the UAS traffic flow is, rather detailing individual aircraft, to spatially aggregate it on a route/area basis, as studied by [6], aimed at urban scenario with a novel lane-based airspace structure. Previous work in this vein for conventional aircraft can be appreciated from [7] which could be used to capture the traffic flow characteristics in a similar way.

The lessons learned from conventional airspace capacity management can be also useful, for instance sector redesign and dynamic sectorisation or flexible opening of predefined airspace configurations. However, in many cases the solutions may not directly apply to U-space, due to their differences in various operational features, even the fundamental airspace structure. In response to this issue, researchers proposed a

This work was partially funded by the SESAR JU under grant agreement No 101017702, as part of the European Union's Horizon 2020 research and innovation programme: AMU-LED (Air Mobility Urban - Large Experimental Demonstrations). The opinions expressed herein reflect the authors view only. Under no circumstances shall the SESAR Joint Undertaking be responsible for any use that may be made of the information contained herein.

wide variety of concepts, such as lanes (corridors) and traffic lights [6], roundabout-like intersections [8], and a comparison via large-scale simulations were conducted by [9] across four concepts involving full-mix, layers, zones and tubes.

More recently, [10] presented a performance-based airspace model, using a set of elementary cells as the reference grid, associated with the UAS protection volume that depends on its CNS (communication, navigation and surveillance) performance. A close framework can be found in DLR (German Aerospace Centre) Blueprint, introducing its concept for urban airspace integration [11]. This Blueprint describes a U-space system enabling dynamic airspace configuration and traffic management. It foresees that the airspace will be segmented into a virtual multi-dimensional map, specifically into cells of similar requirements on airspace usage. Each cell might be used by a few UAS with a large ellipsoid that relies on flight approval, technical capabilities and performance parameters, thus quickly reaching the cell's capacity, or it could be used by more UAS with a smaller ellipsoid.

The fundamental element of DCM is, besides the structured airspace, the flight plans or more precisely the planned UAS trajectories, which is similar as conventional aircraft trajectories to ATFCM (in particular under the paradigm of Trajectory Based Operations). Depending on the user needs, there are various tools available in the market, some of which are integrated with the flight control system, for instance [12]. These tools enable a fast and easy access for average users to plan their flight missions. Generally, they can be considered as the routing or path planning problem, and there have been a wide range of research dedicated to another closely related problem that is trajectory optimisation. An optimal trajectory usually defines a control manoeuvre while satisfying constraints on the kinematics and the dynamics of the vehicle.

The main contributions of this paper are summarised as follows: (1) an integrated DCM approach is proposed, coupling a demand thread (i.e., flight planning management), a capacity thread (i.e., dynamic airspace configuration), and a joint demand-capacity balancing (DCB) thread; (2) a DCB model is presented, optimising the slot allocation, trajectory selection and airspace configuration as a whole; (3) the metrics of both entry count and occupancy are incorporated into the DCB optimisation model as capacity constraint; and (4) a virtual scenario of U-space operations is set up and simulated to evaluate the effectiveness of the proposed approach.

The rest of this paper are organised as follows: Sec. II introduces the functions of UAS flight planning. Sec. III envisions the way how VLL airspace might operate, and thus the expected dynamic capacity management. Then, Sec. IV focuses on the DCB optimisation model which is the core of DCM, supported by alternative trajectory option and dynamic airspace configuration. Numerical experiments are performed in Sec. V through four illustrative examples. Finally, Sec. VI summarises the conclusions and the future work.

II. UAS FLIGHT PLANNING MANAGEMENT

This section introduces a preliminary study for UAS flight planning management, taking into account constraints including the geographical zones, geo-fences and contingency landing sites. This initial study does not compute trajectory of high-fidelity that requires an analysis of vehicle dynamics and performances. The trajectories in this paper only reflect the flight intent, specifically the temporal-spatial traffic demand. However, the proposed DCM approach is generic to have both high- and low-fidelity trajectories as input.

A. Types of operation

According to [13], the planned trajectory might be associated with a "buffer space" because of uncertainties. We can reshape and then group the trajectories into two types, namely *area* and *linear* operations. The difference between the two operations can be noticed from the time and space features of those trajectories. Concretely, with the *area* type of operation, certain positions may be revisited by the UAS for multiple times, while with the *linear* type, it traverses each position for only one time. Based on such classification, we will discuss these two types of trajectories throughout the paper.

B. Geographical zones and geo-fences

The EU Implementing Regulation 2019/947 [14] Article 15 enables the creation of geographical zones (geozones) that restrict access to drones for safety, privacy or environmental reasons. In addition to the geozones (see the yellow circles in Fig. 1) that are more of a strategic (long-term) measure, there is another restriction closer to the short-term phase, namely the geo-fences (see the red rectangles in Fig. 1) that are defined by the (dynamic) geo-fencing service. They are geographic boundaries which should be respected during the UAS operations. For simplicity, this paper considers the time-varying geo-fences based on the operation's planned take-off time, meaning that only those defined at the time when a UAS is scheduled to depart will be taken into account.

C. Contingency/emergency landing sites

Due to operational uncertainties that could lead to undesirable consequences, the UAS operation plan may include contingency or emergency response plans, to be followed in case of unexpected events. These may include alternate landing sites or more complex procedures, as illustrated in [13]. This paper considers the use of alternate landing sites (see the green circles in 1). The planned trajectory will be subject to a constraint that the UAS must remain in range of an adequate landing site at any time through the operation. The idea is to allow the UAS in contingency/emergency to land at a dedicated spot within a certain period of time. For convenience, we use a fixed distance to all these sites, although it may be better to specify a time-based rule.

D. Trajectory generation

Given the above discussion, we then generate the trajectory subject to those constraints. The airspace is mapped by a set of elementary grids. Each grid is connected to its adjacent in 8 directions (except for those on the boundary), and is represented by a central point. Obviously, the more grids we use for a piece of airspace, the more accurately a trajectory can be reflected. We assume a 2D plane in this paper.

To generate the *linear* trajectory, we apply the commonly-used A* algorithm [15], searching for the shortest path composed of a set of sequential grids (see examples with blue curves in Fig. 1). Depending on the buffer space (for uncertainty), additional grids can be included into that sequence. For simplicity, we consider only the original ones (see the blue dots). On top of the fixed path, we then attach the time stamp, starting from a take-off time at its first point, and iterating over each segment given an assumed speed, until reaching the last point for landing time.

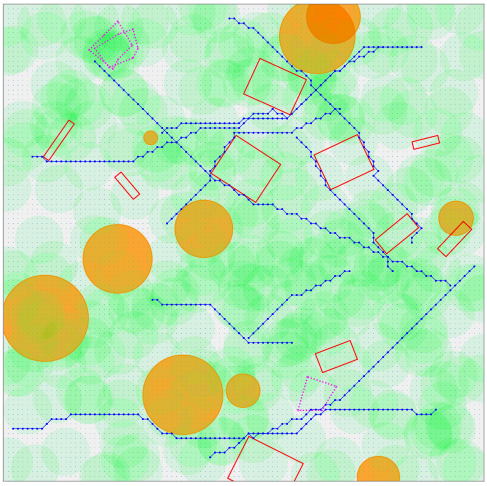

Figure 1: Generated UAS trajectories, involving *linear* trajectories (blue curves), *area* trajectories (purple polygons), geozones (yellow circles), geo-fences (red rectangles) and contingency/emergency landing sites (green areas).

With regard to the *area* trajectory, we consider a (random) set of vertices to define the boundary of an operation. Each edge is similar to the segment of *linear* trajectory, which in turn is subject to all the constraints mentioned above. The major difference lies in their time stamps. Considering that some grids might be revisited from time to time in *area* operations (recall Sec. II-A), we simply set up a unified period of time , rather assigning one time for one grid as done for *linear* operations. In short, there are only two times associated with an *area* trajectory, namely the take-off and landing times that remain the same across all the concerned grids.

III. Dynamic Capacity Management

As foreseen in Swiss U-space, when users are competing for airspace, the DCM service will provide negotiation capabilities and operation planning tools to support collaborative decision making and/or offer alternatives [16]. In this section, we first discuss a primary partition of the VLL airspace into elementary *cells*. Based on that partition, two supporting tools are presented to enable alternative trajectory option (ATO) and dynamic airspace configuration (DAC).

A. VLL airspace partition

In U-space, while the airspace definition and capacity management are still at a very early stage, it is widely recognised that the "full" of an airspace will be related to the probability of flights to lose safe separation [13]. According to the Air-Risk Class proposed by [17], one of the ways to reduce collision risk is to control the geometry of the flights within an airspace. By controlling that through airspace structures, procedures, and regulations, collision risk can be greatly reduced.

Following this thought, it is possible that such geometry parameter may eventually lead to VLL airspace partition. We apply a primary partition by the Voronoi Diagram which is used to divide the airspace into a set of static *elementary* cells. Using this algorithm, a 2D space can be partitioned into convex polygons such that each polygon contains exactly one generating point and every point in a given polygon is closer to its generating point than to any other [18].

Specifically, we also consider the scenario of multiple U-space service providers (USSPs) in a common airspace. As stated in [13], depending on the U-space architecture deployment options and the services, multiple services could be provided by different service providers. It is possible to distinguish between the providers of centralised services (i.e., principle USSP) and concurrent services. As this paper aims at the centralised DCM service, we fully segregate the coverage of each principle USSP.

B. Alternative trajectory option

On top of the fixed *elementary* cells, we then include the previously generated flight trajectories. As shown in Fig. 2, the yellow curve represents an initially planned *linear* trajectory, and the *elementary* cells that this flight is scheduled to traverse are highlighted.

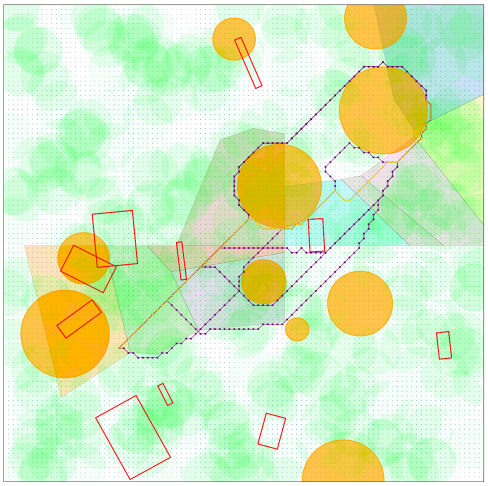

Figure 2: *Linear* operation's alternative trajectory options to route away from each associated *elementary* cell.

Assuming any portion of the airspace becomes full, therefore turning into a hotspot, the flight can route away from the full airspace. In this case, we can generate the rerouting trajectory using the same method when planning the initial trajectory, incorporating additional geographical constraints. Fig. 2 presents all the feasible alternative options (see blue curves) that bypass each of the associated *elementary* cells (except for the ones for take-off and landing).

In addition to the above hotspot-avoidance trajectories, alternatives for any other reason are also applicable, for

instance, a temporal close of airspace. Note that rerouting is not applicable to the *area* operations, meaning that these flights will be subject to only delay regulations.

C. Dynamic airspace configuration

Dynamic capacity management aims to match demand with capacity. In this section, we consider flexibly adjusting *elementary* cells that focuses on the capacity thread. The effects can be two folded: it enables flexible capacity provision in line with demand regulation; and it also adjusts the airspace structure to better accommodate the (regulated) traffic flow.

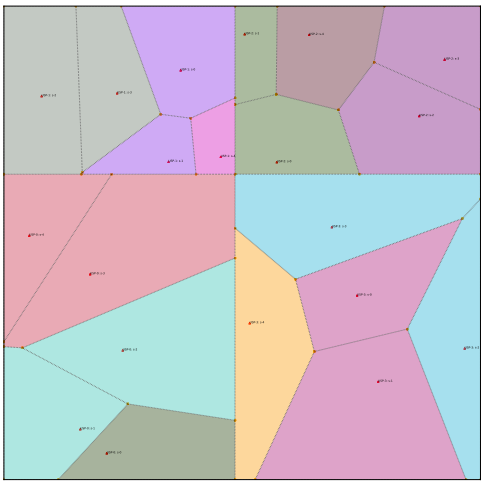

Figure 3: Example of 4 USPs' *configurations*, where the same colour represents one *operational* cell that is composed of one or more *elementary* cells.

First we clarify some airspace relevant concepts used in this paper. The static *elementary* cells resulted from the partition are the basic unit of airspace, which can act individually as one *operational* cell, or can be merged with its adjacent *elementary* cell(s) to act together as another *operational* cell. A combinatorial status for every *elementary* cell of a USSP is referred to as an airspace *configuration*, which could be pre-defined by the USSP.

Fig. 3 shows an example of 4 *configurations* with respect to 4 USPs responsible for that airspace. Obviously, there could be a long list of selectable *configurations* if there exist a large number of *elementary* cells. To make it more realistic, we allow that any adjacent *elementary* cells can be merged, but the maximum number of them within any single *operational* cell is limited.

The capacity of an *operational* cell may depend on various factors, which is why the capacity should be dynamically modified. However, the capacity assessment is beyond the scope of this paper. We assume it is only associated with the size of the area, with a discount factor based on the number of merged *elementary* cells (see details in experimental setup). Regarding capacity counting, we consider the metrics of entry count and occupancy, as will be discussed in the next section.

IV. Demand-capacity balancing model

Given the model input introduced previously in both the demand and capacity threads, along with some assumptions, this section will present the mathematical formulation of the DCB model. It leverages not only conventional slot/delay assignment, but also the alternative trajectory option (ATO) and dynamic airspace configuration (DAC).

A. Decision variables

The model is formulated by mixed integer linear programming and the decision variables are defined below:

$$x_{f,t}^{k,j} = \begin{cases} 1, & \text{if } \textit{linear} \text{ flight } f\text{'s trajectory } k \text{ enters} \\ & \textit{elementary} \text{ cell } j \text{ by time } t \\ 0, & \text{otherwise} \end{cases}$$

$$z_f^k = \begin{cases} 1, & \text{if } \textit{linear} \text{ flight } f\text{'s trajectory } k \text{ is selected} \\ 0, & \text{otherwise} \end{cases}$$

$$y_{a,t}^{en,j} = \begin{cases} 1, & \text{if } \textit{area} \text{ flight } a \text{ enters } \textit{elementary} \text{ cell } j \\ & \text{by time } t \\ 0, & \text{otherwise} \end{cases}$$

$$u_s^\tau = \begin{cases} 1, & \text{if } \textit{configuration } s \text{ is activated in time} \\ & \text{period } \tau \\ 0, & \text{otherwise} \end{cases}$$

Note that if the entrance time for an *area* flight has been determined, the exit time will be known as the flight duration is fixed. Also, once a *configuration* is settled, the status of its associated *operational* cells will be also known. Thus, the following two sets of auxiliary variables are considered:

$$y_{a,t}^{ex,j} = \begin{cases} 1, & \text{if } \textit{area} \text{ flight } a \text{ exits from } \textit{elementary} \\ & \text{cell } j \text{ by time } t \\ 0, & \text{otherwise} \end{cases}$$

$$w_l^\tau = \begin{cases} 1, & \text{if } \textit{operational} \text{ cell } l \text{ is opening in time} \\ & \text{period } \tau \\ 0, & \text{otherwise} \end{cases}$$

Specifically, w_l^τ is equal to $\sum_{s \in S_l} u_s^\tau$, $\forall l \in \mathcal{L}, \forall \tau \in \mathbb{T}$, where S_l is a subset of *configurations* that are composed (partially) of *operational* cell l. In other words, if any *configuration* related with cell l is selected, then this cell must be open; on the contrary, if the cell will not open (i.e. $w_l^\tau = 0$), then all its concerned *configurations* (S_l) cannot be selected.

An important remark and assumption of this model is that, the time period τ to switch among different *configurations* for each USSP, and the rolling time window τ for capturing demand-capacity situations, are synchronised.

B. Objective function

We consider an objective function composed of two parts with respect to demand and capacity respectively, namely the costs of regulating *linear* and *area* flights, and the costs of supplying airspace capacities. In terms of regulating *linear* flights, the costs can be further divided to delay assignment and flight rerouting.

The delay costs for *linear* and *area* flights can be computed by Eqs. 1 and 2 respectively:

$$\sum_{f\in\mathcal{F}}\sum_{k\in\mathcal{K}_f}\sum_{t\in\mathcal{T}_k^{\mathcal{J}_k^{(1)}}}(t-r_k^{\mathcal{J}_k^{(1)}})^{(1+\epsilon)}(x_{f,t}^{k,\mathcal{J}_k^{(1)}}-x_{f,t-1}^{k,\mathcal{J}_k^{(1)}}), \quad (1)$$

$$\sum_{a\in\mathcal{A}}\sum_{t\in\mathcal{T}_a^{\mathcal{J}_a^{(1)}}}(t-r_a^{\mathcal{J}_a^{(1)}})^{(1+\epsilon)}(y_{a,t}^{en,\mathcal{J}_a^{(1)}}-y_{a,t-1}^{en,\mathcal{J}_a^{(1)}}), \quad (2)$$

where $\mathcal{K}_f$ represents a subset of trajectories selectable by *linear* flight f. $\mathcal{T}_k^j, \mathcal{T}_a^j$ are manually defined subsets of time moments feasible for delay assignment (to reduce model dimension), in which j is at position $\mathcal{J}_k^{(1)}, \mathcal{J}_a^{(1)}$ respectively, meaning the first point (based on *elementary* cell) that the trajectory is scheduled to fly over. The initially scheduled times at that positions are presented by $r_k^{\mathcal{J}_k^{(1)}}, r_a^{\mathcal{J}_a^{(1)}}$ respectively. The superlinear coefficient $\epsilon > 0$ for delay costing is used to evenly distribute the delay across different flights.

Next, the costs of rerouting can be denoted by Eq. 3, which is only applicable for the *linear* flights.

$$\sum_{f\in\mathcal{F}}\sum_{k\in\mathcal{K}_f} d_f^k z_f^k, \quad (3)$$

where d_f^k is the additional flight duration of trajectory k compared with the initial duration of *linear* flight f. On the airspace side, the associated service cost is reflected by means of the total amount of capacity provision, namely Eq. 4:

$$\sum_{l\in\mathcal{L}}\sum_{\tau\in\mathbb{T}} c_l^\tau w_l^\tau, \quad (4)$$

where c_l^τ denotes the occupancy capacity supplied through *operational* cell l during the period of time τ.

Finally, the three types of costs are combined as a whole, with weighting cost α set for rerouting, β for delay, and γ for capacity. Also, the flight priority is expressed through a coefficient v_f, v_a to a specific *linear* and *area* flight. The equations can be reorganised as follows:

$$\begin{aligned}\min \sum_{f\in\mathcal{F}}\sum_{k\in\mathcal{K}_f} v_f\Bigg\{&\alpha d_f^k z_f^k+\\ &\sum_{t\in\mathcal{T}_k^{\mathcal{J}_k^{(1)}}}\beta(t-r_k^{\mathcal{J}_k^{(1)}})^{(1+\epsilon)}(x_{f,t}^{k,\mathcal{J}_k^{(1)}}-x_{f,t-1}^{k,\mathcal{J}_k^{(1)}})\Bigg\}+\\ &\sum_{a\in\mathcal{A}}\sum_{t\in\mathcal{T}_a^{\mathcal{J}_a^{(1)}}} v_a\beta(t-r_a^{\mathcal{J}_a^{(1)}})^{(1+\epsilon)}(y_{a,t}^{en,\mathcal{J}_a^{(1)}}-y_{a,t-1}^{en,\mathcal{J}_a^{(1)}})+\\ &\sum_{l\in\mathcal{L}}\sum_{\tau\in\mathbb{T}}\gamma c_l^\tau w_l^\tau,\end{aligned} \quad (5)$$

The constraints are listed below, which can be grouped into individual flight operations, airspace configurations, and traffic entry count/occupancy capacity, as well as the binary condition and space of the decision variables.

C. Individual flight operations

Below constraints are associated with the operational limits with regard to each individual *linear* or *area* flight.

$$\text{s.t.} \quad \sum_{k\in\mathcal{K}_f} z_f^k = 1 \quad \forall f\in\mathcal{F}, \quad (6)$$

$$x_{f,\underline{\mathcal{T}}_k^j-1}^{k,j}=0,\ x_{f,\overline{\mathcal{T}}_k^j}^{k,j}=z_f^k \quad \forall f\in\mathcal{F},\forall k\in\mathcal{K}_f,\forall j\in\mathcal{J}_k, \quad (7)$$

$$\begin{aligned}y_{a,\underline{\mathcal{T}}_a^j-1}^{en,j}=y_{a,\underline{\mathcal{T}}_a^j+\hat{t}_a-1}^{ex,j}=0,\ y_{a,\overline{\mathcal{T}}_a^j}^{en,j}=y_{a,\overline{\mathcal{T}}_a^j+\hat{t}_a}^{ex,j}=1\\ \forall a\in\mathcal{A},\forall j\in\mathcal{J}_a,\end{aligned} \quad (8)$$

$$x_{f,t}^{k,j}-x_{f,t-1}^{k,j}\geq 0 \quad \forall f\in\mathcal{F},\forall k\in\mathcal{K}_f,\forall j\in\mathcal{J}_k,\forall t\in\mathcal{T}_k^j, \quad (9)$$

$$\begin{aligned}y_{a,t}^{en,j}-y_{a,t-1}^{en,j}\geq 0,\ y_{a,t+\hat{t}_a}^{ex,j}-y_{a,t+\hat{t}_a-1}^{ex,j}\geq 0\\ \forall a\in\mathcal{A},\forall j\in\mathcal{J}_a,\forall t\in\mathcal{T}_a^j,\end{aligned} \quad (10)$$

$$\begin{aligned}x_{f,t+\hat{t}_k^{jj'}}^{k,j'}-x_{f,t}^{k,j}=0 \quad \forall f\in\mathcal{F},\forall k\in\mathcal{K}_f,\forall t\in\mathcal{T}_k^j, j=\mathcal{J}_k^{(i)},\\ j'=\mathcal{J}_k^{(i+1)}:\forall i\in[1,n),\end{aligned} \quad (11)$$

$$\begin{aligned}y_{a,t}^{en,j'}-y_{a,t}^{en,j}=0 \quad \forall a\in\mathcal{A},\forall t\in\mathcal{T}_a^j, j=\mathcal{J}_a^{(i)},\\ j'=\mathcal{J}_a^{(i+1)}:\forall i\in[1,n),\end{aligned} \quad (12)$$

$$y_{a,t+\hat{t}_a}^{ex,j}-y_{a,t}^{en,j}=0 \quad \forall a\in\mathcal{A},\forall j\in\mathcal{J}_a,\forall t\in\mathcal{T}_a^j, \quad (13)$$

Constraint 6 states that only one trajectory, among all options, can be selected for each *linear* flight. This constraint is then linked with Constraint 7. They specify that, if a trajectory is selected (i.e. $z_f^k=1$) then it must be assigned with a slot from the set of $\mathcal{T}_k^j$, otherwise (i.e. $z_f^k=0$) no slot will be assigned. There is no alternative trajectory option for *area* flight, so Constraint 8 enforces that a slot will be assigned at each point. Specifically, as the flight duration $\hat{t}_a$ is fixed, the lower and upper bound of feasible time moments at the "exit" point can be expressed by $\underline{\mathcal{T}}_a^j+\hat{t}_a$ and $\overline{\mathcal{T}}_a^j+\hat{t}_a$, where $[\underline{\mathcal{T}}_a^j, \overline{\mathcal{T}}_a^j]$ are the feasible time moments defined at the "entrance" point.

Constraints 9 and 10 enforce the continuity of the timeline (recall the concept of *by* time). Constraint 11 stipulates that the controlled flight time between any segment (j, j') of a *linear* flight, remain unchanged than initially scheduled. In the meantime, Constraint 12, with respect to the *area* flight, enforces the controlled times to be the same at all cells covered by that flight. Constraint 13 shows that the duration of any *area* flight does not change from the initially planned.

D. Airspace configurations

The two constraints cover the opening of *operational* cells across the airspace, which is realised by means of selecting (and thus scheduling) a number of pre-defined *configurations*:

$$\sum_{s\in\mathcal{S}_u} u_s^\tau = 1 \quad \forall u \in \mathcal{U}, \forall \tau \in \mathbb{T}, \tag{14}$$

$$\sum_{s\in S_l} u_s^\tau = w_l^\tau \quad \forall l \in \mathcal{L}, \forall \tau \in \mathbb{T}, \tag{15}$$

Constraint 14 states that only one *configuration* can be selected during each period of time, where $\mathcal{S}_u$ represents the set of selectable options of *configurations* defined beforehand by the USSP u. Constraint 15 links the selection of *configuration* and the opening of *operational* cell, as explained previously in Sec. IV-A with regard to the auxiliary variables.

E. USSP entry count capacity

As a mature and widely-recognised definition of VLL airspace capacity has not reached yet, in this paper we consider to reuse two well-studied metrics in ATM, including entry count and occupancy. Their comparison has been clarified in [19]. Concretely, the entry count is adopted as the measure of USSP's capacity, specifying how many UAS are allowed to enter into a USSP's coverage within a certain period of time. The occupancy is meanwhile used as the measure of the *operational* cell's capacity, specifying how many UAS are allowed to appear in a smaller cell's coverage within a certain period of time.

$$\begin{aligned}&\sum_{f\in\mathcal{F}}\sum_{k\in\mathcal{K}_f}\sum_{t\in\tau\cap\mathcal{T}_k^{\mathcal{J}_u}}(x_{f,t}^{k,\mathcal{J}_u}-x_{f,t-1}^{k,\mathcal{J}_u})\\ &+\sum_{a\in\mathcal{A}}\sum_{t\in\tau\cap\mathcal{T}_a^{\mathcal{J}_u}}(y_{a,t}^{en,\mathcal{J}_u}-y_{a,t-1}^{en,\mathcal{J}_u})\le c_u^\tau \quad \forall u\in\mathcal{U},\forall\tau\in\mathbb{T},\end{aligned} \tag{16}$$

Constraint 16 states that the number of UAS entries into each USSP must be lower than its capacity in any times. Note that this involves both *linear* and *area* flights, and the coverage and shape of USSP will remain unchanged. One major concern of this metric is that the exit time, upon UAS entering a piece of airspace, will not be taken into account. However, the duration of internal movement may still pose workload on the U-space service provision.

F. Cell occupancy capacity

For the occupancy metric, to formalise the calculation, we stipulate that one occupancy will be added, only if the AND condition is satisfied: the flight's entry time is earlier than (or equal to) the period's ending moment, and also the flight's exit time is later than (or equal to) the period's starting moment.

The main barrier of performing that calculation lies in the judgement of the relationship between a controlled (entrance/exit) time and a period (starting/ending) boundary. Concretely, the feasible time moments $(\mathcal{T}_k^j, \mathcal{T}_a^j)$ will be limited (if compared with the whole time horizon) so as to reduce the dimension of the model.

Therefore, we need a group of helper variables to conduct that judgement. Specifically, $m_{f,\tau}^{k,j'}, n_{f,\tau}^{k,j}$ are defined for the *linear* flights, while $p_{a,\tau}^j, q_{a,\tau}^j$ for the *area* flights. $n_{f,\tau}^{k,j}, q_{a,\tau}^j$ represent if the controlled time of flight (k or a) entering cell j is earlier than (or equal to) the ending moment $\overline{\tau}$ of period τ. On the contrary, $m_{f,\tau}^{k,j'}, p_{a,\tau}^j$ denote if the controlled time of flight (k or a) leaving from cell j is later than (or equal to) the starting moment $\underline{\tau}$ of period τ. Cell j' used in *linear* flight f represents the next consecutive cell j to be flown by trajectory k, thus entering cell j' means leaving from cell j. The helper variables can be computed via Eq. 17:

$$\begin{cases} m_{f,\tau}^{k,j'} &= \sum\limits_{t\in[\underline{\tau},\overline{\mathcal{T}}_k^{j'}]\cap\mathcal{T}_k^{j'}}(x_{f,t}^{k,j'}-x_{f,t-1}^{k,j'})\\ n_{f,\tau}^{k,j} &= \sum\limits_{t\in[\underline{\mathcal{T}}_k^{j},\overline{\tau}]\cap\mathcal{T}_k^{j}}(x_{f,t}^{k,j}-x_{f,t-1}^{k,j})\\ p_{a,\tau}^{j} &= \sum\limits_{t\in[\underline{\tau},\overline{\mathcal{T}}_a^{j}]\cap\mathcal{T}_a^{j}}(y_{a,t+\hat{t}_a}^{ex,j}-y_{a,t+\hat{t}_a-1}^{ex,j})\\ q_{a,\tau}^{j} &= \sum\limits_{t\in[\underline{\mathcal{T}}_a^{j},\overline{\tau}]\cap\mathcal{T}_a^{j}}(y_{a,t}^{en,j}-y_{a,t-1}^{en,j}) \end{cases} \tag{17}$$

The main idea is to capture the relationship between two boundaries: the bounds of feasible time moments ($\mathcal{T}_k^j$ or $\mathcal{T}_a^j$) and the period's boundaries ($\underline{\tau}$ and $\overline{\tau}$).

Using the above helper variables, we can then compute the occupancy with the left-hand part of Constraint 18:

$$\begin{aligned}&\sum_{f\in\mathcal{F}}\sum_{k\in\mathcal{K}_{f,\tau}^{j,j'}:j=\underline{\mathcal{J}}_k^l,j'=\overline{\mathcal{J}}_k^l}(m_{f,\tau}^{k,j'}+n_{f,\tau}^{k,j}-z_f^k)+\\ &\sum_{a\in\mathcal{A}_\tau^j:j=\underline{\mathcal{J}}_a^l}(p_{a,\tau}^j+q_{a,\tau}^j-1)\le c_l^\tau w_l^\tau+(1-w_l^\tau)M\\ &\qquad\qquad\qquad\qquad\forall l\in\mathcal{L},\forall\tau\in\mathbb{T},\end{aligned} \tag{18}$$

where an additional scalar of -1 needs to be further included (recall the AND condition, where only 1 occupancy will be added provided both conditions are met). For the *linear* flights, however, a trajectory k can be either selected, so that this -1 should be associated to z_f^k.

With regard to the subsets $k\in\mathcal{K}_{f,\tau}^{j,j'}, a\in\mathcal{A}_\tau^j$ in Constraint 18, the period of counting occupancy will roll over the whole time horizon, but it is not necessary to, at each period, look through all flights (or trajectories). The two subsets are therefore used to exclude flights (or trajectories) that are never going to appear in the target period. This will help significantly reduce the model's dimension.

As for the right-hand part of Constraint 18, unlike the fixed coverage considered for each USSP (recall Constraint 16), the actual capacity provision of an *operational* cell l depends on if it is actually opened during period τ. If so, $w_l^\tau = 1$, then the declared capacity c_l^τ has to be respected; otherwise $w_l^\tau = 0$, this Constraint will be relaxed (as M is a large positive number that always makes it feasible).

Worth noting that, while the occupancy metric has been widely adopted in post-regulation DCB performance assessment, it is the first time, to the best of our knowledge, that this metric is used as a pre-regulation constraint in a

DCB optimisation model. Further added to the value, it is considered in a context of dynamic airspace configuration.

G. Decision variables conditions

$$x_{f,t}^{k,j} \in \{0,1\} \quad \forall f \in \mathcal{F}, \forall k \in \mathcal{K}_f, \forall j \in \mathcal{J}_k, \forall t \in \mathcal{T}_k^j, \quad (19)$$

$$z_f^k \in \{0,1\} \quad \forall f \in \mathcal{F}, \forall k \in \mathcal{K}_f, \quad (20)$$

$$y_{a,t}^{en,j}, y_{a,t+\hat{t}_a}^{ex,j} \in \{0,1\} \quad \forall f \in \mathcal{F}, \forall j \in \mathcal{J}_a, \forall t \in \mathcal{T}_a^j, \quad (21)$$

$$u_s^\tau \in \{0,1\} \quad \forall s \in \mathcal{S}, \forall \tau \in \mathbb{T}, \quad (22)$$

$$w_l^\tau \in \{0,1\} \quad \forall l \in \mathcal{L}, \forall \tau \in \mathbb{T}. \quad (23)$$

Finally, Constraints 19 - 23 state the binary constraints and domains of the primary and auxiliary decision variables used in the model.

V. Illustrative examples

This section presents the numerical experiments, where we build up an illustrative U-space scenario. The airspace covers a 2D space of $20 * 20$ km^2, divided by $100 * 100$ grids (being each grid of $0.2 * 0.2$ km^2). Four case studies have been considered, switching on/off certain DCB initiatives, including delay assignment, ATO and DAC. Results are compared across these cases to demonstrate their impacts on demand-capacity balancing and associated operating costs.

A. Experimental setup

As shown in Fig. 4, the traffic sample includes 296 flights (285 *linear* and 14 *area*) throughout the 6 hours' overall duration. It appears 10 geographical zones, 10 geo-fences and 350 landing sites (with a fixed range of 1 km) across this airspace. The initially generated trajectories can be seen in Fig. 4a. Meanwhile, 4 principle USSPs are involved to provide services independently, partitioning each one's coverage into 7 *elementary* cells (see Fig. 4b).

Next, the trajectory and cell intersections can be derived. In average, a *linear* trajectory traverses 4.9 *elementary* cells, concerning 2 USSPs, while an *area* trajectory covers 1.6 *elementary* cells, involving 1 USSP. Then, we notice that for each *linear* trajectory, it has an average of 3.1 alternative options (a maximum of 10 is seen in a few cases), which sums up to 890 alternative trajectory options in total.

Regarding airspace structure, we set 4 as the maximum number of *elementary* cells that can be merged as one *operational* cell. Accordingly, the 28 *elementary* cells are combined into 247 different *operational* cells, each of which is associated with a particular capacity of occupancy. Furthermore, each USSP has approximately 237 selectable *configurations* (total 949 for the airspace) in each period of time. Apart from the assumptions mentioned in Sec. II and III, additional key assumptions have been made in the experiments:

- The DCB unit time step is 1 min and the DCB time window is considered as per 20 min (thus 18 periods within the whole duration);
- The weighted costs concerning flight priority (i.e. v_f, v_a) are randomly generated between $[1, 10]$, and the fairness factor (ϵ) is set to 0.05;
- The cost of delay (β) is 1 per minute; the cost of extra flight time due to rerouting (α) is 4 per minute; and the cost of providing a single occupancy capacity (γ) is 0.1 per 20 min;
- The occupancy capacity (per 20 min) is linearly correlated with the size of *elementary* cell, with a coefficient of 0.5 ac/km^2, but it reduces exponentially by 0.6^{n-1}, where $n \in [2, 4]$ is the number of *elementary* cells in an *operational* cell;
- The entry count capacity (per 20 min) is linearly correlated with the size of USSP's coverage, with a coefficient of 0.125 ac/km^2; and
- The speeds of *linear* operations are randomly selected between 10-50 m/s, and the durations of *area* operations are randomly set between 5-30 minutes.

B. Case studies

We consider four case studies, with or without ATO/DAC, as listed in Table I. The DCB model presented in Sec. IV can be customised to realise each of these cases. Specifically, the proposed model represents Case-D; by disabling ATO (enforcing $z_f^{\mathcal{K}_f} = 1, \ \forall f \in \mathcal{F}$), or disabling DAC (enforcing $w_l^\tau = 1, \ \forall l \in \mathcal{L}^{(1)}, \forall \tau \in \mathbb{T}$, where $\mathcal{L}^{(1)}$ is a subset of *operational* cells that are composed of only one *elementary* cell), we can obtain Case-B and Case-C respectively; and by disabling both, we derive Case-A, where delay remains the only option. In any case, delaying the take-off time will be always available.

TABLE I. Cases switching on/off ATO and DAC.

Case	Delay	ATO	DAC
Case-A	√	–	–
Case-B	√	–	√
Case-C	√	√	–
Case-D	√	√	√

Given the experience gained from our numerical experiments, we observe that the amount of delay needed in different Cases vary significantly. As a consequence, we set different values with respect to the length of $\mathcal{T}_f^j, \mathcal{T}_a^j$ that will determine the maximum allowed delay per flight, namely Case-A: 180 min, Case-B: 45 min, Case-C: 20 min, Case-D: 15 min. Note that this does not "manipulate" the results, as the actual delay is much lower than the given bound. However, this largely reduces the dimension of the optimisation model, thus can improve computational efficiency.

In this study, GAMS v.25.1 software suite has been used as the modelling tool and Gurobi v.7.5 optimiser as the solver. The experiments have been run on a 64 bit Intel® Core™ i7-8700 CPU @ 3.20GHz 6 Cores computer with 32 GB of RAM and Linux OS.

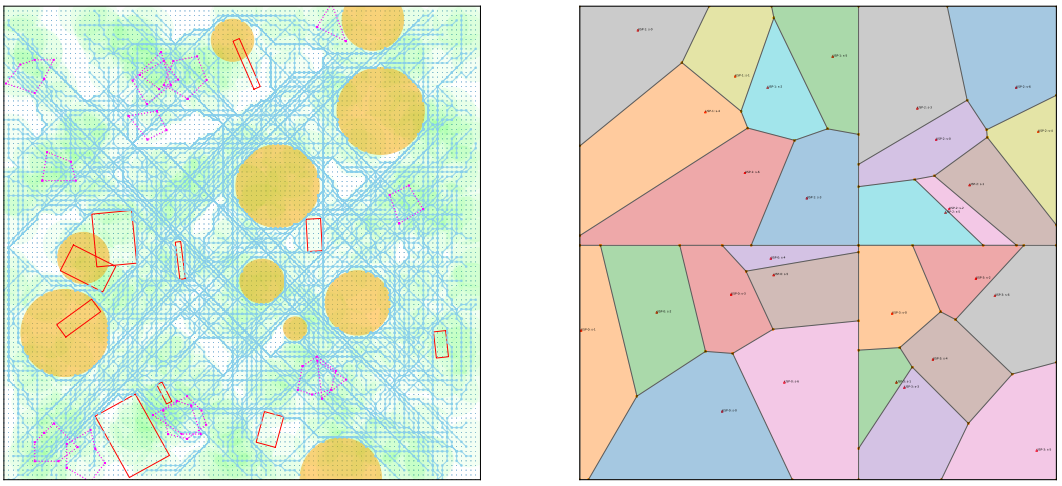

(a) Planned UAS trajectories involving *linear* trajectories (blue curves) and *area* trajectories (purple polygons)

(b) Partitioned airspace cells (4 USSPs each with 7 cells)

Figure 4: Initialisation of an illustrative U-space scenario of this study.

C. Demand and capacity balances

The demand and capacity consequences are presented with regards to the above Cases (post-regulation), as well as the original situation (pre-regulation). The USSP entry count capacity and the cell occupancy capacity are both assessed. Fig 5 shows the original, Case-A, and other more advanced cases. In the original case, no regulation has been imposed and every single *elementary* cell acts as the *operational* cell. The USSP's coverage, thus capacity, remains constant, so it is represented by a horizontal line in Fig. 5a. There are 124 (7*18) *operational* cells opened throughout the 18 periods of time, whose capacity also remains constant during the 18 periods, as shown in Fig. 5b. Obviously, some capacity overloads (i.e. demand higher than capacity) can be observed, which is more severe against the cell occupancy.

By means of assigning delays in Case-A, all the capacity overloads can be effectively mitigated as shown in Figs. 5c and 5d. However, as the target time horizon covers only 6 hours' time, there might be a notable amount of demand to be moved out of the horizon provided their assigned delay is large enough. Such propagated demand will also affect the capacity in other periods, thus incurring additional delay than what is shown in this study.

In Case-B, a notable difference than the previous is that the number of opened *operational* cells is significantly less (see Fig. 5f), as some *elementary* cells are merged into one single *operational* cell. This is because, with a fixed airspace structure, the capacity provision might be not distributed properly (recall the majority unoccupied capacities in Fig. 5d). Allowing dynamic airspace configuration will however enable the available (reduced although) capacity to be better utilised (see the minority unoccupied capacities in Fig. 5f). As such, less delay is required to meet the cell capacity, which also affects the USSP entry count, as shown in Fig. 5e). Namely, the exceeded demand will not have to be always delayed towards the end of the horizon, but instead can be distributed more evenly within the periods.

Figs. 5g and 5h present the situation in Case-C, where the airspace structure remains unchanged but we allow UAS to reroute away from the overloaded cells. This is realised by incorporating a set of alternative trajectory options submitted by each flight beforehand. Note that this set of trajectories involve all potential rerouting options bypassing each cell that it originally traverses. The effects are obvious, namely the demand can be redistributed not only in temporal (by means of delay), but also in spatial to less congested areas.

Based on the above discussion, we may notice that Case-B and Case-C essentially have only improved the regulation of Case-A from one thread, either demand or capacity. Finally, Case-D deals with both threads at the same time (see Fig. 5i and 5j). As such, the decisions with regards to rerouting and airspace adjustment, along with delay assignment, can be achieved in a more synchronised way. Compared with Case-B, the amount of opened *operational* cells (and thus the capacity provision) can be further reduced in Case-D. In the meantime, the required amount of delay also decreases, which will be discussed next.

D. Result comparisons

A detailed comparison in some key performance indicators (KPIs) across the cases can be seen in Table II. The KPIs are divided into various areas, including delay, rerouting, demand, capacity, DC (demand/capacity) ratio, and solution.

We can observe that a huge amount of delay (8,098 min), being 42% flights (123) affected, is required in Case-A, if considering that the capacity overloads seem only mild (recall 5a and 5f). For Case-B and Case-C, the required delay reduces significantly to 226 min and 132 min, which suggests the effectiveness of ATO and DAC in delay reduction. The ATO seems more efficient, but it incurs some extra costs when diverting flights elsewhere, whereas DAC saves costs by means of reconfiguring the opened cells. In Case-D, their synthetic effects are revealed, with the numbers of both delay and cells further lowed down. What is more, less amount of

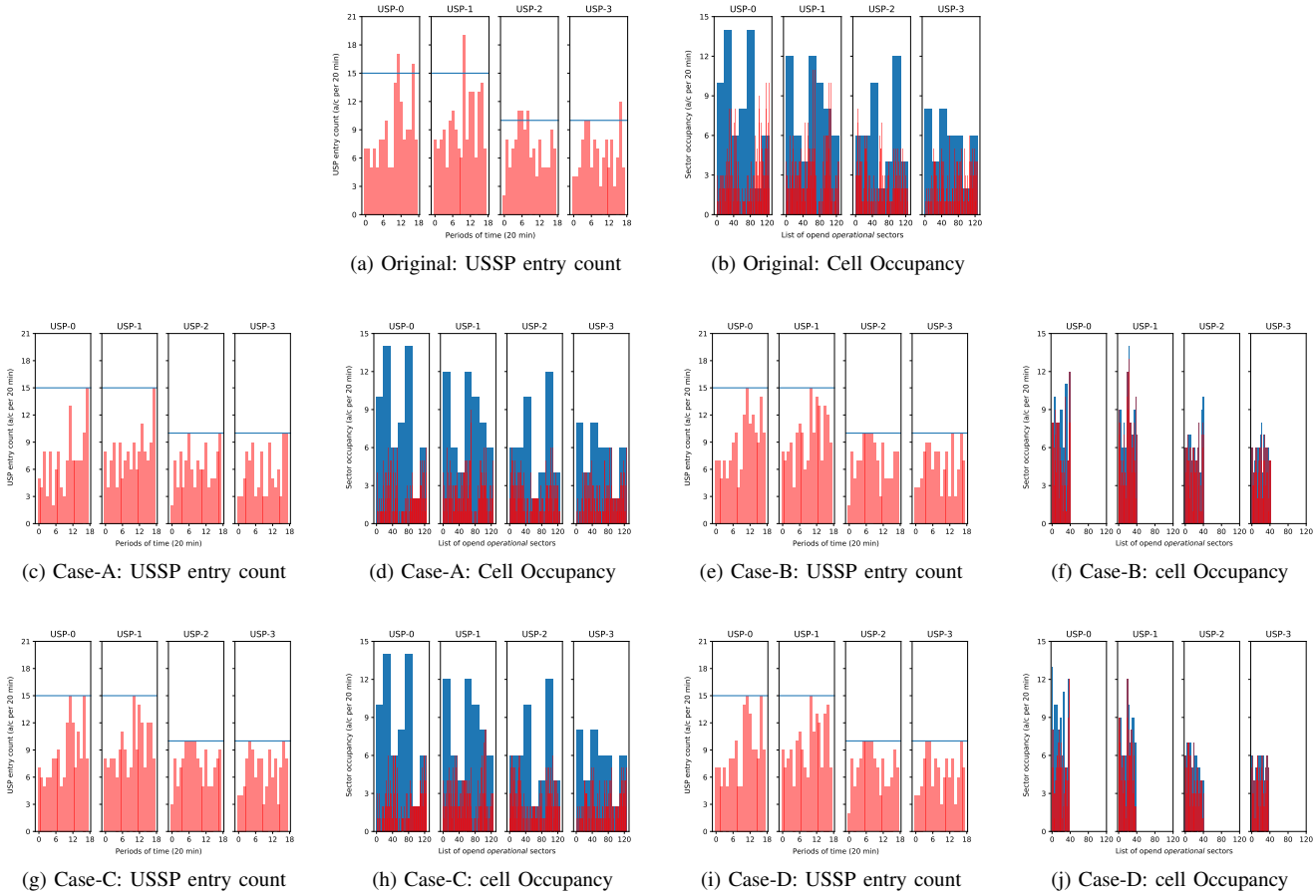

(a) Original: USSP entry count (b) Original: Cell Occupancy

(c) Case-A: USSP entry count (d) Case-A: Cell Occupancy (e) Case-B: USSP entry count (f) Case-B: cell Occupancy

(g) Case-C: USSP entry count (h) Case-C: cell Occupancy (i) Case-D: USSP entry count (j) Case-D: cell Occupancy

Figure 5: Demand (red bars), USSP entry count capacity (blue lines) and *operational* cell occupancy capacity (blue bars), with respect to the original and other Cases.

TABLE II. Result comparisons across four Cases of the study.

KPI	**Case-A**	**Case-B**	**Case-C**	**Case-D**
Delay (min)-*linear*	8,053	201	124	42
Delayed flights (a/c)-*linear*	121	36	27	13
Delay (min)-*area*	45	25	8	8
Delayed flights (min)-*area*	2	3	2	2
Initial trajectory (#)	285	285	187	209
Alternative trajectory (#)	0	0	98	76
USSP entry count-pre (a/c)	578	578	578	578
USSP entry count-post (a/c)	479	578	578	578
Cell occupancy-pre (a/c)	1,249	1,249	1,249	1,249
Cell occupancy-post (a/c)	1,042	879	1,074	744
USSP capacity provision (a/c)	900	900	900	900
Cell capacity provision (a/c)	3,600	1,154	3,600	1,054
Opened *operational* cells (#)	504	166	504	157
USSP DC ratio-pre (%)	64.2	64.2	64.2	64.2
USSP DC ratio-post (%)	53.2	64.2	64.2	64.2
Cell DC ratio-pre (%)	34.7	34.7	34.7	34.7
Cell DC ratio-post (%)	28.9	76.2	29.8	70.6
Solution gap (%)	0	1	0	0
Solution time (sec)	8	1,874	2	127

rerouting ATO is needed (i.e., from 98 in Case-C to 76 in Case-D), meaning less extra costs for the flights.

As previously mentioned, the effects of DAC are two folded, enabling airspace structure adjustment plus flexible capacity provision. The former will affect the demand to be counted against occupancy (recall Sec. IV-F). As some *elementary* cells are merged into larger cells, part of the boundary crossings are regarded as internal movements, thus reducing the total number of occupancy (e.g. 879 in Case-B) as presented in Table II. However, such cell merging cannot always continue, as the combined capacity declines with the number of *elementary* cells involved, and thus the accumulated demand will quickly reach the capacity. The reduction of occupancy in Case-A is simply due to the fact that some demand has been delayed out of the target horizon. In Case-B and Case-D, we can observe that rerouting ATO can also contribute to the occupancy reduction.

The latter effect in flexible capacity provision has been reflected in Fig. 5. A large amount of capacity that is originally planned yet not fully used can be removed or reallocated to where/when it is needed. For this reason, the provided cell capacity can be lowered down to 1,154 in Case-B and further to 1,054 in Case-D, whereas the original plan is 3,600. This can be also appreciated by the increased DC ratios (namely the cell loads) in Table II. Without DAC, such ratios are less than 30%, but with DAC they can be improved remarkably to more than 70%.

Remember in Sec. III-A the original plan is simply to open all the *elementary* cells that are generated randomly. A more

sophisticated pre-planning, given the estimated flight demand, can be done, which is exactly what Case-B does. Thus, Case-B might be regarded as airspace planning. Based on that, the subsequent ATO can be planned more efficiently. There will be a clearer information of potential hotspots to avoid, rather than bypassing any *elementary* cell that any flight traverses.

Finally, the solution quality and speed across different Cases are also shown in Table II. Considering the dimension and complexity of the problems, the computational performance seems acceptable (due to the model formulation), except for Case-B that is a bit under satisfactory. In light of our experimental experience, the most challenging decision part is on DAC, followed by delay assignment and ATO.

VI. Conclusions and further work

In this paper, we demonstrated an integrated approach aimed at shaping the service of Dynamic Capacity Management (DCM) in future U-space operations. The approach couples the modules of flight planning, airspace configuration and demand-capacity balancing optimisation. A simulation scenario under the proposed framework was set up to perform a group of case studies. Results proved that the integration is promising as it achieves the best outcome if comparing with other cases where module functions are partially decoupled.

The approach covers a wide range of aspects in U-space, and we acknowledge that the development of specific modules is still at an initial stage. Some critical questions remain open. In terms of flight planning management, how to incorporate high-fidelity trajectory computation (e.g., 4D trajectory with wind impact) and collaborative decision making mechanisms (for fairness concerns) into the DCM service are some important questions. With regard to airspace management, the fundamental structure may need attention, along with the capacity prediction, dynamically modification and configuration adjustment, just to name a few, on top of that airspace structure. As for demand-capacity balancing, we may further consider what could be the potential solutions in response to non-nominal uncertainties and how to associate the solutions with flight planning and airspace management. These are some directions that deserve exploring in our future work.

References

[1] SESAR, "European drones outlook study, unlocking the value for europe," SESAR JU, Tech. Rep., 2016.

[2] ——, "European ATM master plan: Roadmap for the safe integration of drones into all classes of airspace," SESAR JU, Tech. Rep., 2018.

[3] C. Chin, K. Gopalakrishnan, A. Evans, M. Egorov, and H. Balakrishnan, "Tradeoffs between efficiency and fairness in unmanned aircraft systems traffic management," in *Proceedings of the 9th International Conference on Research in Air Transportation (ICRAT)*, Castelldefels, Catalonia, Spain, 2020.

[4] D. Bertsimas and S. Gupta, "Fairness and collaboration in network air traffic flow management: an optimization approach," *Transportation Science*, vol. 50, no. 1, pp. 57–76, 2015.

[5] H. Balakrishnan and B. Chandran, "A distributed framework for traffic flow management in the presence of unmanned aircraft," in *Proceedings of the 12th USA/Europe Air Traffic Management Research and Development Seminar (ATM2017)*, Seattle, Washington, US, 2017.

[6] D.-S. Jang, C. A. Ippolito, S. Sankararaman, and V. Stepanyan, "Concepts of airspace structures and system analysis for uas traffic flows for urban areas," in *AIAA Information Systems-AIAA Infotech @ Aerospace*, Grapevine, Texas, US, 2017, p. 0449.

[7] A. M. Bayen, R. L. Raffard, and C. J. Tomlin, "Eulerian network model of air traffic flow in congested areas," in *Proceedings of the 2004 American Control Conference*, vol. 6. Boston, MA, US: IEEE, 2004, pp. 5520–5526.

[8] D. Sachatny and T. C. Henderson, "A lane-based approach for large-scale strategic conflict management for uas service suppliers," in *Proceedings of the 2019 International Conference on Unmanned Aircraft Systems (ICUAS)*. Atlanta, GA, US: IEEE, 2019, pp. 937–945.

[9] J. M. Hoekstra, J. Ellerbroek, E. Sunil, and J. Maas, "Geovectoring: reducing traffic complexity to increase the capacity of uav airspace," in *Proceedings of the 8th International Conference on Research in Air Transportation (ICRAT)*, Castelldefels, Catalonia, Spain, 2018.

[10] N. Pongsakornsathien, S. Bijjahalli, A. Gardi, A. Symons, Y. Xi, R. Sabatini, and T. Kistan, "A performance-based airspace model for unmanned aircraft systems traffic management," *Aerospace*, vol. 7, no. 11, p. 154, 2020.

[11] DLR, "DLR Blueprint: Concept for Urban Airspace Integration - Integrating UAS into the future aviation system, a flexible approach enabling large-scale UAS operations," Institute of Flight Guidance, Tech. Rep. Version 1.0, 2017.

[12] DJI, "DJIFlightPlanner," 2020. [Online]. Available: https://www.djiflightplanner.com

[13] CORUS, "U-space concept of operations," SESAR JU, Tech. Rep. Edition 03.00.02, 2019.

[14] European Commission, "Commission implementing regulation (EU) 2019/947 on the rules and procedures for the operation of unmanned aircraft," European Union, Tech. Rep. 2019/947, 2019.

[15] P. E. Hart, N. J. Nilsson, and B. Raphael, "A formal basis for the heuristic determination of minimum cost paths," *IEEE transactions on Systems Science and Cybernetics*, vol. 4, no. 2, pp. 100–107, 1968.

[16] FOCA, "Swiss u-space conops version 1.1," Federal Office of Civil Aviation (FOCA) and the Swiss U-Space Implementation (SUSI) Public-Private Partnership, Tech. Rep. COO.2207.111.2.3742183, 2020.

[17] JARUS, "JARUS guidelines on specific operations risk assessment (SORA)," Joint Authorities for Rulemaking of Unmanned Systems, Tech. Rep. Edition 1.0, 2020.

[18] F. Aurenhammer and R. Klein, "Voronoi diagrams." *Handbook of computational geometry*, vol. 5, no. 10, pp. 201–290, 2000.

[19] EUROCONTROL, "Hourly entry count versus occupancy count relationship definitions and indications (i)," EUROCONTROL Experimental Centre, Tech. Rep. EEC Note No. 15/07, 2007.

Biographies

Ms Yiwen Tang is currently a PhD candidate in Aerospace theme at Cranfield University. She received her MSc in Air Transport Management from Cranfield University in 2019, and MSc and BEng from Nanjing University of Aeronautics and Astronautics in 2020 and 2016. Her main research interests include ATM/UTM integration. Email address: yiwen.tang@cranfield.ac.uk

Dr Yan Xu is a Lecturer in ATM/CNS with the Centre for Autonomous and Cyber-Physical Systems in the School of Aerospace, Transport and Manufacturing at Cranfield University. He received his Ph.D. in Aerospace Science and Technology from the Technical University of Catalonia, and received his M.Sc. and B.Eng. in Traffic Engineering from Nanjing University of Aeronautics and Astronautics. His main research interests include air traffic flow and capacity management, ATM/UTM and Urban Air Mobility. Email address: yanxu@cranfield.ac.uk

Prof Gokhan Inalhan is BAE Systems Chair, Professor of Autonomous Systems and Artificial Intelligence and Deputy Head of Autonomous and Cyber-physical Systems Centre at Cranfield University. He has previously served as Director General of ITU Aerospace Research Centre. He has published over 200 papers, book chapters, proceedings and technical reports on advanced controls, optimisation and modelling aspects associated with autonomy and artificial intelligence for air, space, defence and transportation systems (UAM, ATM/UTM) with seminal works on multiple aircraft coordination and decentralised control of Unmanned Aerial Systems (UASs). Email address: inalhan@cranfield.ac.uk

Prof Antonios Tsourdos is a Professor of autonomous systems and control at Cranfield University, appointed Head of the Autonomous and Cyber-Physical Systems Centre in 2007 and Director of Research for the School of Aerospace, Transport and Manufacturing in 2015. He is the editorial board member on several international publications. He has been involved in a number of research projects on UTM including ASTRAEA, U-Space funded project EuroDrone, and DfT funded project UTM Open Access and EPSRC funded project CASCADE. He has published a number of papers on topics related to UTM including assured autonomy, sense and avoid, networking UAS. Email address: a.tsourdos@cranfield.ac.uk